Eur. Phys. J. B **42**, 165–173 (2004)
DOI: 10.1140/epjb/e2004-00368-5

THE EUROPEAN PHYSICAL JOURNAL B

Dielectric resonance, local field distribution, and optical response in 3D resonant composites

B. Dai, Y. Gu[a], C. Li, and Q.-H. Gong[b]

State Key Laboratory for Mesoscopic Physics, Department of Physics, Peking University, Beijing 100871, P.R. China

Received 29 June 2004 / Received in final form 19 August 2004
Published online 14 December 2004 –

Abstract. We extend the Green's function formalism in a binary 2D composite to 3D. Using the formalism, we investigate the dielectric resonances, local-field distribution, and effective linear optical responses for one-bond, two-bond and three-bond clusters, as well as for various disordered composites. Due to the different values of Green's function in 2D and 3D, for the same cluster, the values of the dielectric resonances in 3D are smaller than those in 2D, but the fields are more localized than those in 2D. The sum rule of dielectric resonance in three-component composites is extended to d dimensions. For the same resonance, the intensity of the local-field in 3D is also weaker than that in the 2D case, but the fields are more localized than those in 2D. For the disordered composites in 2D and 3D, inverse participation ratios (IPR) with $q = 2$ are used to represent the localization of the field. When we increase the concentration of impurity bonds, a blue shift of IPR peaks occurs in 3D, while in 2D, these peaks are very stable. Finally, both for 2D and 3D disordered composites, the absorption range broadens with increasing impurity concentration, and a red shift of the absorption peak is observed in 3D.

PACS. 77.84.Lf Composite materials – 42.65.-k Nonlinear optics

1 Introduction

Recently, resonant properties of composite materials have attracted great interest. Composites with impurity bonds embedded in a dielectric host were examined. For such composites, the local-field distribution has been widely studied; it is known that the local field is extremely inhomogeneous in the volume around the metallic clusters [1]. Various eigenmode localizations, such as the localized dipolar excitation on roughly nanostructured surfaces [2], the surface-plasmon modes in disordered nanosystems [3–5], and the selective photomodification in fractal aggregates of colloidal particles [6], are highly sensitive to the specific local-field distribution when resonance takes place [7,8,20]. Moreover, the experiment has been carried out on such composites [9], and a large infrared absorption was observed [10,11]. The metallic clusters show a strong non-linear optical response when they are structured on the nanoscale, through the geometric resonance and local-field effects [12,13]. The relevant linear and nonlinear optical responses in composites were reported to be strongly enhanced due to a great fluctuation of local fields [4,14–16].

There are various methods for computing the effective conductivity of composites materials [17]. The effective-medium theory [18] (EMT) was extended to the nonlinear response of percolating composites and fractal clusters to avoid numerical difficulty. For linear problems, EMT usually captures the kernel; while for nonlinear problems, it reduces the local-field fluctuation, leading to results that may not be quite accurate. The developed Green's function formalism (GFF) [19] can be used to calculate the dielectric resonance, local-field distribution in binary and multi-component composites [14,20,21], and optical response of dilute isotropic and anisotropic composites [22]. Currently, the GFF, however, is only concerned with a 2D model; while a 3D model may be more fundamental in that it could be applied to more realistic systems. Meanwhile, although there exists a method [23] dealing with the dielectric resonance in 3D disordered media, it is not valid for the local-field distribution and optical response. Motivated by that, we have extended the existing GFF in 2D [19,21] to 3D composites.

The arrangement of this paper is as follows. In Section 2, the Green's function of a 3D finite-difference Laplace operator on the cubic lattice is worked out, and the electrostatic Green's function of the clusters subject to a point source in a 3D network is given. In Section 3, the dielectric resonance of one-bond and two-bond metallic clusters with various geometric configurations in 3D composites is calculated and compared with that of the corresponding clusters in 2D. It is found that, for the same cluster, the values of the dielectric resonances in 3D are smaller than those found in 2D, due to the different values

[a] e-mail: ygu@pku.edu.cn
[b] e-mail: qhgong@pku.edu.cn

of Green's function. The sum rule of dielectric resonance in three-component composites becomes: $\sum s_m = \frac{n_2}{d}\eta + \frac{n_1}{d}$, where d is the degree of dimensionality, $\eta(=\frac{\epsilon_2-\epsilon_0}{\epsilon_1-\epsilon_0})$ the difference admittance ratio, and n_1 and n_2 the number of two kinds of impurity bonds with the admittance ϵ_1 and ϵ_2. In Section 4, for one-bond and two-bond clusters, we investigate the local-field distribution near resonance, as well as the inverse participation ratio (IPR), which is used to represent the localization of the field. For the same resonance, the intensity of the local-field in 3D is weaker than that in the 2D case. When the concentration of impurity bonds increases, a blue shift of IPR's peak occurs in 3D, while in 2D, it is almost stable. This could be attributed to different Green's functions between the 3D and 2D networks. In Section 5, the effective linear optical responses concerning disordered media are studied. Both for 2D and 3D disordered composites, the absorption range broadens with increasing impurity concentration. And we find a red shift of the absorption peak in 3D. Finally, in Section 6, we summarize the whole work.

2 Green's function formalism in 3D composites

2.1 Green's function of 3D finite-difference Laplace operator $\triangle$

Green's function of the 3D finite-difference Laplace operator $\triangle$ on the cubic lattice is the basis for the following calculation. The Green function $G_{\vec{x},\vec{y}} = G(\vec{x}-\vec{y})$ is defined by the solution of

$$-\triangle G(\vec{x}) = \delta_{\vec{x},\mathbf{0}} \tag{1}$$

with $\delta_{\vec{x},0}$ being the Kronecker symbol. The difference equation has a unique solution with all required symmetries, up to an additive constant, which we fix by setting $G(\mathbf{0}) = 0$. We acquire by Fourier transformation that [24]

$$G_{\vec{x},\vec{y}} = G(x_1-y_1,x_2-y_2,x_3-y_3) = \int_B \frac{d^3p}{(2\pi)^3}\frac{e^{i\vec{p}\cdot(\vec{x}-\vec{y})}-1}{K(\vec{p})} \tag{2}$$

(p_1, p_2, and p_3 being the three ordinates of $\vec{p}$) where the three integral runs over the first Brillouin zone $B(-\pi < p_1, p_2, p_3 < \pi)$. According to the definition of the finite-difference operator on 3D cubic lattice

$$-\triangle G(\vec{x}) = \sum_{i=1}^{3}[-G(x_i+1) + 2G(x_i) - G(x_i-1)], \tag{3}$$

with the shift theorem of Fourier transformation, we obtain the Fourier transformation of $-\triangle$

$$K(\vec{p}) = 2(3 - \cos p_1 - \cos p_2 - \cos p_3). \tag{4}$$

Via a complex integral, the solution of $G(\vec{x})$ can finally be recast as

$$G(\vec{x}) = \frac{1}{48\pi^3}\int_B \frac{1-\cos(x_1p_1+x_2p_2+x_3p_3)}{1-\frac{1}{3}(\cos x_1+\cos x_2+\cos x_3)}, \tag{5}$$

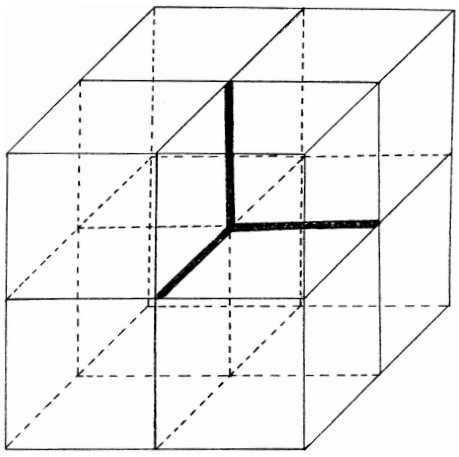

Fig. 1. Schematic diagram of a cluster (shown by the thick lines) embedded in a three dimensional infinite cubic network.

in line with the result of reference [24]. Although Green's function $G(\vec{x})$ in a 3D network is quite similar to that in 2D [25], the properties of the solutions are quite different. Let r be the distance between a site and the point source. For Green's function of the 3D finite-difference Laplace operator, the value of G diminishes to $-\infty$ when $r \to \infty$ with a rate of $\frac{1}{r}$, and the network is transient, while for 2D Green's function, the rate is $\ln r$, and the network is recurrent [25,26]. Moreover, the values of Green's function in 3D are comparatively smaller than the 2D case for the same r.

2.2 Green's function formalism for a binary composite in 3D network

In this part, we extend the former work [19,21] concerning the electrostatic Green's function of the clusters subject to a point source in a 2D infinite square network to the 3D case. Consider a 3D cubic network in which impurity bonds of admittance ϵ_1 are employed to replace bonds of the otherwise homogeneous network of identical admittance ϵ_0 (see Fig. 1). We define a cluster as a finite set of impurity bonds on the lattice. And our purpose is to find the Green function of the impurity clusters subject to a point source, which can be used to compute the resonant properties by the principle of superposition. GFF in 3D is different from that in 2D merely in the values of Green's function.

Suppose a unit point source is placed at site $\mathbf{0} = (0,0,0)$ outside a set of clusters of n_s sites. The electric potential V satisfies the Kirchhoff equation

$$\sum_{\vec{\mathbf{y}}(\vec{\mathbf{x}})} \epsilon_{\vec{\mathbf{x}},\vec{\mathbf{y}}}(V_{\vec{\mathbf{x}},\mathbf{0}} - V_{\vec{\mathbf{y}},\mathbf{0}}) = \delta_{\vec{\mathbf{x}},\mathbf{0}}, \tag{6}$$

where $\vec{\mathbf{x}} = (x_1, x_2, x_3)$ and $\vec{\mathbf{y}}(\vec{\mathbf{x}})$ denotes the six nearest neighboring sites of $\vec{\mathbf{x}}$; $V_{\vec{\mathbf{x}},\mathbf{0}}$ is the electrostatic Green's function at $\vec{\mathbf{x}}$ due to the point source and $\epsilon_{\vec{\mathbf{x}},\vec{\mathbf{y}}} = \epsilon_{\vec{\mathbf{y}},\vec{\mathbf{x}}}$ is the admittance of the bond joining the neighboring sites $\vec{\mathbf{x}}, \vec{\mathbf{y}}$.

Let $v = 1 - \epsilon_1/\epsilon_0$, equation (6) can be recast as [19]

$$-\Delta V_{\vec{\mathbf{x}},\mathbf{0}} = v \sum_{\vec{\mathbf{y}} \in C(\vec{\mathbf{x}})} (V_{\vec{\mathbf{x}},\mathbf{0}} - V_{\vec{\mathbf{y}},\mathbf{0}}) + \delta_{\vec{\mathbf{x}},\mathbf{0}}/\epsilon_0 \tag{7}$$

where the notation $\vec{\mathbf{y}} \in C(\vec{\mathbf{x}})$ means that the bond $(\vec{\mathbf{x}}, \vec{\mathbf{y}})$ belongs to the set C of clusters, and Δ denotes the finite difference Laplace operator on the cubic lattice as

$$-\Delta F_{\vec{\mathbf{x}}} \equiv \sum_{\vec{\mathbf{y}}(\vec{\mathbf{x}})} (F_{\vec{\mathbf{x}}} - F_{\vec{\mathbf{y}}}) \tag{8}$$

for any physical value $F_{\vec{\mathbf{x}}}$. Equation (7) admits a formal solution

$$V_{\vec{\mathbf{x}},\mathbf{0}} = \frac{G_{\vec{\mathbf{x}},\mathbf{0}}}{\epsilon_0} + v \sum_{\vec{y} \in C} \sum_{\vec{\mathbf{x}} \in C(y)} G_{\vec{\mathbf{x}},\vec{\mathbf{y}}} (V_{\vec{\mathbf{y}},\mathbf{0}} - V_{\vec{\mathbf{x}},\mathbf{0}}). \tag{9}$$

Then equation (9) can be simplified by defining a matrix M

$$M_{\vec{\mathbf{x}},\vec{y}} = \sum_{\vec{\mathbf{z}} \in C(\vec{\mathbf{y}})} (G_{\vec{\mathbf{x}},\vec{y}} - G_{\vec{\mathbf{x}},\vec{z}}) \tag{10}$$

so that

$$V_{\vec{\mathbf{x}},\mathbf{0}} = \frac{G_{\vec{\mathbf{x}},\mathbf{0}}}{\epsilon_0} + v \sum_{\vec{y} \in C} M_{\vec{\mathbf{x}},\vec{y}} V_{\vec{y},\mathbf{0}}. \tag{11}$$

The first term of the right-hand side of equation (11) is the unperturbed Green's function of a point source at site $\mathbf{0}$ in the absence of the clusters, and the second term describes the perturbation caused by the clusters. And M is generally an $\infty \times n_s$ matrix for an infinite network while V and G are column vectors of the Green's functions.

2.3 Solution for dielectric resonance and local-field distribution

Let $\tilde{M}, \tilde{V}$,and $\tilde{G}$ denote the values in the clusters subspace; $\tilde{M}$ is an $n_s \times n_s$ submatrix of M, while $\tilde{V}$ and $\tilde{G}$ are confined to the n_s cluster sites. As discussed in reference [19], by transformation, at any site $\vec{\mathbf{x}}$ the potential $V_{\vec{x},\mathbf{0}}$ can be expressed by equation (11). For $\vec{\mathbf{x}} \in C$, equation (11) becomes

$$\tilde{V}_{\vec{\mathbf{x}},\mathbf{0}} = \frac{\tilde{G}_{\vec{\mathbf{x}},\mathbf{0}}}{\epsilon_0} + v \sum_{y \in C} \tilde{M}_{\vec{\mathbf{x}},\vec{y}} \tilde{V}_{\vec{y},0}. \tag{12}$$

that can be rewritten as

$$\sum_{\vec{y} \in C} [\tilde{\delta}_{\vec{x},\vec{y}} - v\tilde{M}_{\vec{x},\vec{y}}] V_{\vec{y},0} = \frac{\tilde{G}_{\vec{x},0}}{\epsilon_0} \tag{13}$$

which can be readily be inverted to yield $\tilde{V}$, by solving a set of n_s simultaneous linear equations. Substituting the solution of equation (13) into equation (11), the Green's function of all sites in the lattice can be obtained and the geometric resonance is characterized by a nontrivial solution of equation (13). In this case, the electric potential around the clusters can be expressed in terms of the eigenvectors of the normal mode. And the nontrivial eigenvalues correspond to real physical resonances.

Let $s = \epsilon_0/(\epsilon_0 - \epsilon_1) = 1/v$, the n_R real eigenvalues of $\tilde{M}$ share the same range of $0 \le s \le 1$ with the 2D case. For a particular eigenvalue of $\tilde{M}$, the corresponding right and left eigenvectors are denoted by $\tilde{R}_m$ and $\tilde{L}_m$. We write $\tilde{V}$ as a linear combination of the eigenvectors $\tilde{R}$. According to references [19,21], for $x \in C$,

$$\tilde{V} = \sum_{n=1}^{n_R} \frac{s}{\epsilon_0 (s - s_n)} \left(\sum_{\vec{\mathbf{y}} \in C} \tilde{L}_{n,\mathbf{y}} \tilde{G}_{\mathbf{y},0} \right) \tilde{R}_n \tag{14}$$

and when s is very close to s_m, the local field distribution could be identified by the residue of $\tilde{V}_{x,0}$ as

$$\begin{aligned} \text{Residue}(\tilde{V}_{\vec{x},0}) &= \lim_{s \to s_m} (s - s_m) \tilde{F}_{\vec{x},0} \\ &= \frac{s_m}{\epsilon_0} \tilde{R}_{m,x} \left(\sum_{\vec{\mathbf{y}} \in C} \tilde{L}_{m,y} \tilde{G}_{\mathbf{y},0} \right) \end{aligned} \tag{15}$$

while for $x \notin C$,

$$\begin{aligned} V_{\vec{\mathbf{x}},\mathbf{0}} = \frac{G_{x,0}}{\epsilon_0} + \frac{1}{\epsilon_0} \sum_{n=1}^{n_R} \frac{s}{(s - s_n)} \left(\sum_{\vec{\mathbf{y}} \in C} \tilde{L}_{n,y} \tilde{G}_{y,0} \right) \\ \times \left(\sum_{\mathbf{y} \in C} M_{x,z} \tilde{R}_{n,z} \right) \end{aligned} \tag{16}$$

and

$$\text{Residue}(V_{\vec{\mathbf{x}},\mathbf{0}}) = \frac{1}{\epsilon_0} \left(\sum_{\vec{\mathbf{y}} \in C} \tilde{L}_{m,\mathbf{y}} \tilde{G}_{\mathbf{y},0} \right) \left(\sum_{\mathbf{z} \in C} M_{x,z} \tilde{R}_{m,z} \right). \tag{17}$$

Compared with reference [19], equations (14–17) share the same form those for the 2D case. Therefore, when $\vec{\mathbf{x}}$ is outside the cluster, both the point source and the polarization of the clusters contribute to the Green's function; while when inside, only the polarization contributes.

3 Dielectric resonances

The dielectric resonances of the one-bond, two-bond and three-bond metallic clusters embedded in a dielectric host are studied. All topologically different clusters with one bond, various connected two-bond and three-bond clusters are shown in Figure 2, where the three-bond cluster in 3D has two additional different spatial structures (3f and 3g) than that in 2D networks (Ref. [27]). The dielectric resonances are shown in Table 1, with s_m being the nontrivial eigenvalue of $\tilde{M}$. From this table, it is found that the resonances distribute in the range of $0 \le s_m \le 1$ and there are n nontrivial eigenvalues corresponding to n bonds, which are the same for 2D and 3D. For the same configuration, the values of the resonances in 3D are comparatively smaller than those in 2D: take cluster 2a for example, in 3D, the two eigenvalues are 0.45682 and 0.20984, while for 2D, the corresponding eigenvalues

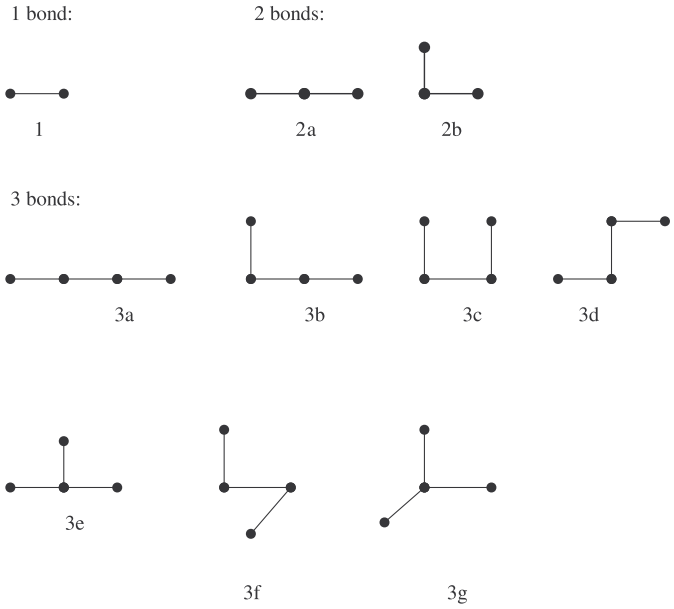

Fig. 2. All topologically different clusters with one bond, two bonds, and three bonds embedded in a three dimensional cubic lattice.

are 0.63662 and 0.36338. Such results originate in the difference of Green's function in 2D and 3D mentioned in Section 2.

It is found that for a cluster with n bonds in 2D, the summation of the dielectric resonances obeys a sum rule:

$$\sum s_m = \frac{n}{2}; \tag{18}$$

while for 3D case,

$$\sum s_m = \frac{n}{3}. \tag{19}$$

The relationships have been proved for various binary systems [14]. Moreover, it has been numerically proved [28] that for the three-component composite the relationship is: $\sum s_m = \frac{n_2}{2}\eta + \frac{n_1}{2}$with the total impurity bonds $n = n_1 + n_2$ and $\eta(= \frac{\epsilon_2 - \epsilon_0}{\epsilon_1 - \epsilon_0})$ being the difference admittance ratio; therefore, such a sum rule can be extended to the 3D case:

$$\sum s_m = \frac{n_2}{3}\eta + \frac{n_1}{3}. \tag{20}$$

Without loss of generality, this sum rule becomes

$$\sum s_m = \frac{n_2}{d}\eta + \frac{n_1}{d} \tag{21}$$

where d is the spatial dimension. And we always use it to check the numerical calculations.

4 Local-field distribution and inverse participation ratios with q = 2

4.1 Local-field distribution near resonance

To illustrate the general formalism, we will compute the electric potential V for one-bond and various two-bond clusters. Recent numerical simulation on random impedance network [29] has shown that in the limit of a small volume fraction of metallic bonds, the optical absorption spectrum is dominated by isolated clusters of a few bonds. We also compare its localization with what has been found in 2D composites.

Table 1. Values of dielectric resonance for the simple metallic clusters with one bond, two and three bonds embedded in the infinite cubic and square dielectric lattice.

Lattice	s(3D)	Summation of s(3D)	s(2D)	Summation of s(2D)
1	0. 333333	1/3	0. 5	1/2
	0. 456825	2/3	0. 63662	1
2a	0. 209842		0.36338	
	0. 469127	2/3	0. 68169	1
2b	0. 19754		0. 31831	
	0. 494615		0. 67136	
	0. 361164	1	0. 54648	3/2
3a	0. 144221		0. 28216	
	0. 50538		0. 707136	
	0. 357137	1	0. 543158	3/2
3b	0. 137483		0. 249706	
	0. 496968		0. 697564	
	0. 395079	1	0. 63662	3/2
3c	0. 107953		0. 165816	
	0. 519656		0. 553491	
	0. 344946	1	0. 553491	3/2
3d	0. 135398		0. 229264	
	0. 596803		0. 834184	
	0. 209842	1	0. 36338	3/2
3e	0. 193355		0. 302436	
	0. 515986			
	0. 352593	1		
3f	0. 131421		~~NONE~~	~~NONE~~
	0. 604921			
	0. 19754	1		
3g	0. 19754			

4.1.1 One-bond cluster

For a single bond placed from site $(1, 0, 0)$ to site $(2, 0, 0)$ as shown in Figure 1, with a point source placed at site $(0, 0, 0)$, the submatrix $\tilde{M}$ reads

$$\tilde{M} = \begin{pmatrix} G_{0,0} - G_{1,0} & G_{1,0} - G_{0,0} \\ G_{1,0} - G_{0,0} & G_{0,0} - G_{1,0} \end{pmatrix} \tag{22}$$

where $G_{0,0} = 0$ and $G_{1,0} = -\frac{1}{6}$. There is a nontrivial eigenvalue [24] $s = \frac{1}{3}$, and the normalized right and left eigenvectors of this eigenvalue are

$$\tilde{R}_1 = \left(\frac{1}{\sqrt{2}}, -\frac{1}{\sqrt{2}}\right)^T, \tilde{L}_1 = \left(\frac{1}{\sqrt{2}}, -\frac{1}{\sqrt{2}}\right). \tag{23}$$

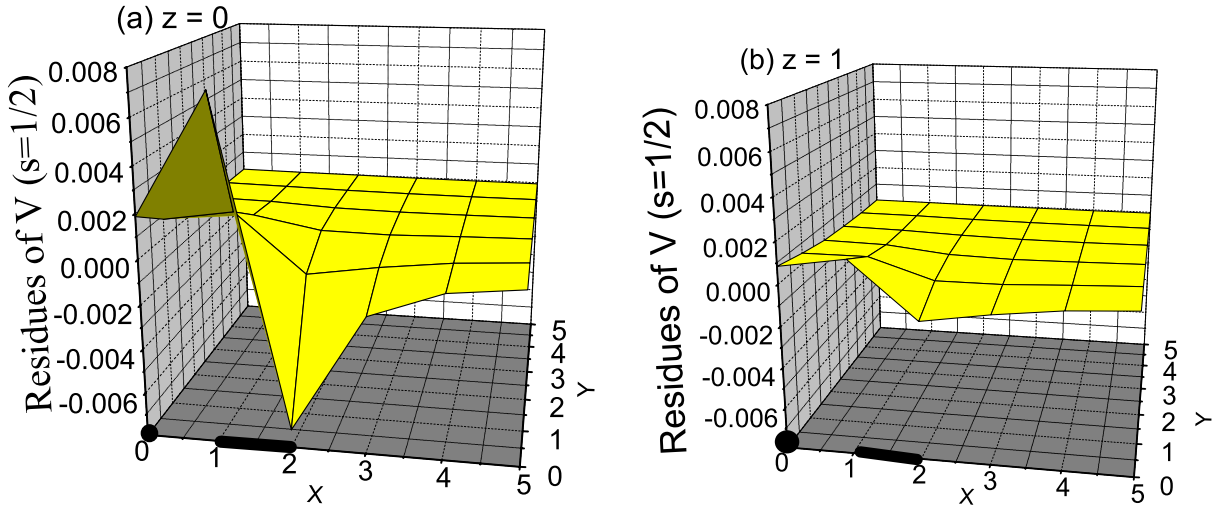

Fig. 3. Residues of the 3D Green's function around the one-bond cluster placed from $(1,0,0)$ to $(2,0,0)$ with $s = 1/3$. (a) $z = 0$ plane; (b) $z = 1$ plane.

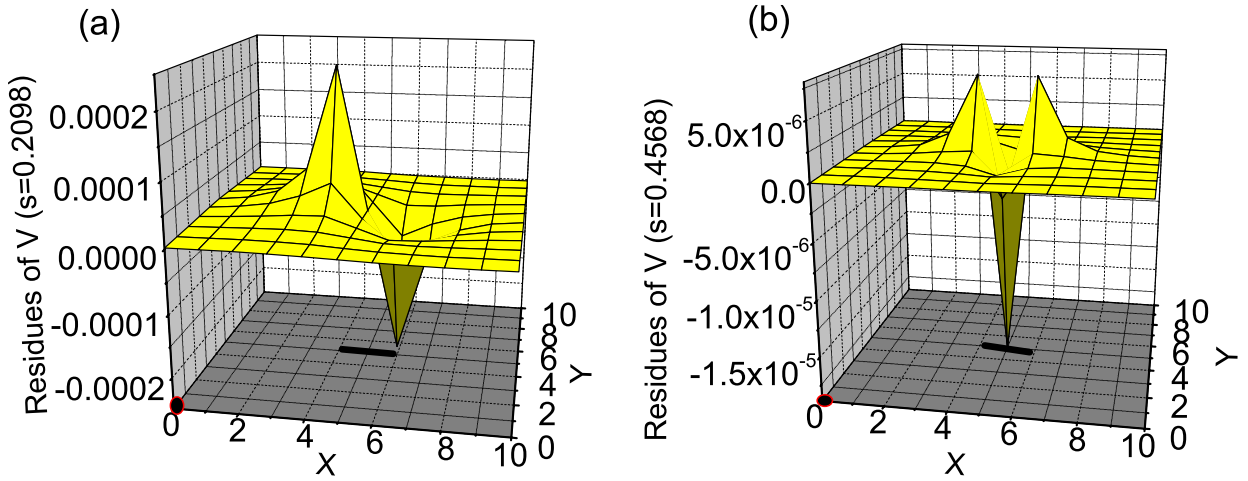

Fig. 4. Residues of the 3D Green's function around a linear cluster from site $(4,5,0)$ via $(5,5,0)$ to site $(6,5,0)$ at the $z = 0$ plane. The linear cluster is shown as a thick line. (a) $s = 0.2098$; (b) $s = 0.4568$.

Let $\epsilon_0 = 1$.When $\vec{\mathbf{x}} \in C$, the residue of the Green's function of the one-bond cluster can be written as

$$\begin{aligned}\text{Residue}(\tilde{V}_{\vec{\mathbf{x}}}) &= \lim_{s\to 1/3}\left(s-\frac{1}{2}\right)\tilde{F}_x \\ &= s_1\tilde{R}_{1,x}\left(L_{1,1}\tilde{G}_1 + \tilde{L}_{1,2}\tilde{G}_2\right) \end{aligned} \quad (24)$$

where $G_2 = -0.2098$. Therefore

$$\text{Residue}(\tilde{V}_1) = 0.007196, \text{Residue}(\tilde{V}_2) = -0.007196. \quad (25)$$

When $\vec{\mathbf{x}} \notin C$, we get

$$\text{Residue}(V_{\vec{\mathbf{x}}}) = \frac{1}{\epsilon_0}(\tilde{L}_{1,1}G_1 + \tilde{L}_{1,2}G_2)(M_{x,1}\tilde{R}_{1,1} + M_{x,1}\tilde{R}_{1,2}) \quad (26)$$

since the local field distribution is symmetric about the bond, we only show the result of the Green's function on the right-hand side of the bond.

Figure 3 displays the 3D plot of the residue at the $z = 0$ and $z = 1$ plane ($X - Y$ plane) around a one-bond cluster placed from $(1,0,0)$ to $(2,0,0)$ (shown by the thick line) subject to a unit positive point source at $(0,0,0)$. As is evident from Figure 3, there is a strong dipolar response along the bond at resonance with a node at the mid point of the cluster. Such a localization becomes much weaker at $z = 1$, i.e., it diminishes rapidly with the distance, indicating that the field at resonance is strongly localized around the cluster. Compared with former work [19], it is clear that the local-field distribution for a one-bond cluster in both a 2D square lattice and a 3D cubic lattice has a similar behavior. Generally, the intensity of local field in a 2D lattice is comparatively larger than that in a 3D lattice, namely, the intensity of the peak is about 0.030 for 2D while less than 0.008 for 3D, due to the different values of Green's function in 2D and 3D.

4.1.2 Two-bond clusters

Now we will give examples of two-bond clusters. For simplicity, only the 3D plots in the $z = 0$ plane are given. Figure 4 shows the residues near resonances around a linear cluster (Type-2a in Fig. 2) placed from site $(4,5,0)$

$$p = \frac{p_1 l_1(l_2+1)(l_3+1) + p_2 l_2(l_1+1)(l_3+1) + p_3 l_3(l_1+1)(l_2+1)}{l_1(l_2+1)(l_3+1) + l_2(l_1+1)(l_3+1) + l_3(l_1+1)(l_2+1)}, \tag{29}$$

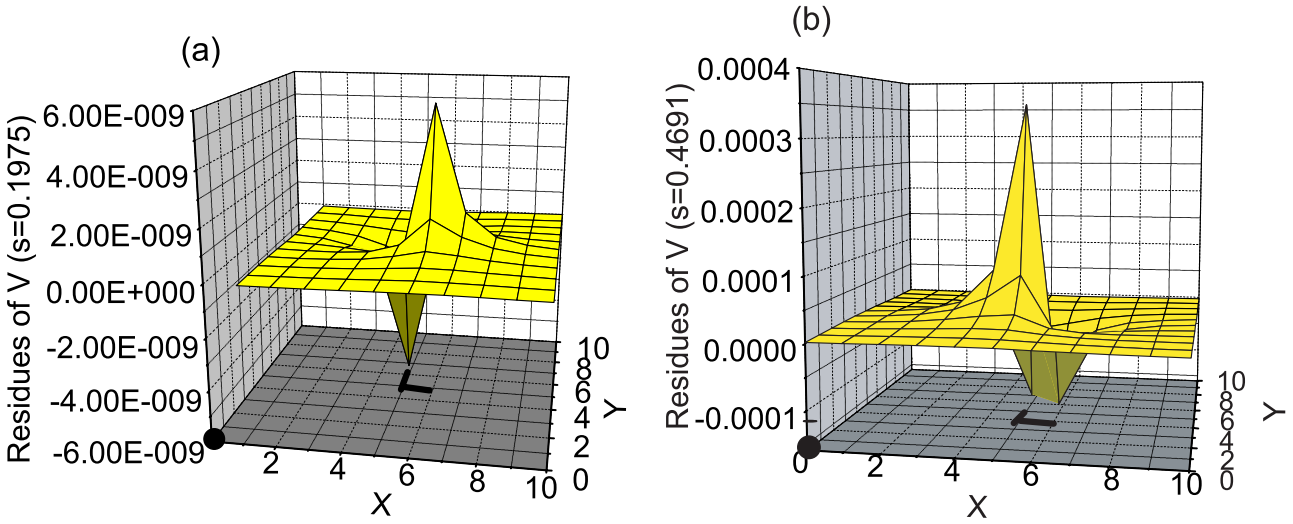

Fig. 5. Residues of the 3D Green's function around a corner cluster from site $(5, 6, 0)$ via $(5, 5, 0)$ to site $(6, 5, 0)$ at the $z = 0$ plane. The corner cluster is shown as a thick line. (a) $s = 0.1975$; (b) $s = 0.4691$.

via $(5, 5, 0)$ to $(6, 5, 0)$ (shown by the thick line) subject to a unit positive point source placed at $(0, 0, 0)$, and in the $z = 0$ plane. For type-(2a), when $s = 0.2098$, which is smaller than the eigenvalue of a single bond $s = \frac{1}{3}$, the results are similar to those of the one-bond case, namely, there is a strong and localized dipolar response with a node at the middle site of the cluster (Fig. 4a). When $s = 0.4568$ (greater than $\frac{1}{3}$), however, there is an antinode at the middle site of the cluster. Compared with 2D case [19], it is evident that the shape of local-field distribution are the same, while the intensity of the response becomes weaker because of different values of Green's function in 2D and 3D.

Figure 5 describes the residues near resonances around a cluster (type-2b in Fig. 2) placed from site $(5, 6, 0)$ via $(5, 5, 0)$ to $(6, 5, 0)$ in the $z = 0$ plane. When $s = 0.1975$, as shown in Figure 5a, the results are similar to the one-bond case but its dipolar response is the inverse of that of the one-bond case. When $s = 0.4691$, as shown in Figure 5b, there is a strong but asymmetric dipolar response. The results are also compared with the corresponding 2D case [19]. It can be concluded that a given cluster mainly determines the shape of the local-field distribution near resonances while the values of Green's function decides the intensity of the response.

4.2 Inverse participation ratios with q = 2 in random binary resonant composites

The nth normalized right eigenvector is

$$R_n = \{R_{n,1}, R_{n,2}, \cdots, R_{n,i} \cdots R_{n,n_s}\} \tag{27}$$

with n_s being the number of sites that belong to clusters, and $\langle R_n^2 \rangle = 1$. The IPR of R_n is defined as [22,30]

$$\mathrm{IPR}(R_n) = \sum_{i=1}^{n_s} R_{n,i}^{2q} \tag{28}$$

where $q = 2$. The calculation of $\mathrm{IPR}(R_n)$ is confined within the nontrivial eigenstates. According to equations (16) and (17), the right eigenvectors of $\tilde{M}$ are closely related to the local fields of the impurity cluster in the subspace. So the IPR can be used to represent the localization of the eigenstates by amplifying the outline of eigenstates, namely, the localized states become more pronounced and extended states become smoother. Therefore, the larger values of IPR always correspond to the stronger optical responses. This will be verified in the following.

In this part, we will study the IPR in 3D disordered binary composites by comparing with the IPR of 2D composites. Let p_1, p_2, and p_3 represent the concentration of impurity bonds in the three directions in a given sample area. For simplicity, we set $p_1 = p_2 = p_3$. Then the volume fraction p of the given composites is

see equation (29) above

l_1, l_2 and l_3 are the number of bonds in the three directions. In this problem, we simply set $l_1 = l_2 = l_3$, so $p = p_1 (= p_2 = p_3)$. Figure 6 illustrates the size effect of IPR. Here $p = 0.2$, and the sample size is from $7 \times 7 \times 7$ to $8 \times 8 \times 8$. Comparing Figure 6a with Figure 6b, we find that the distributions of IPR have similar features: the localized states are inclined to accumulate when s nearly

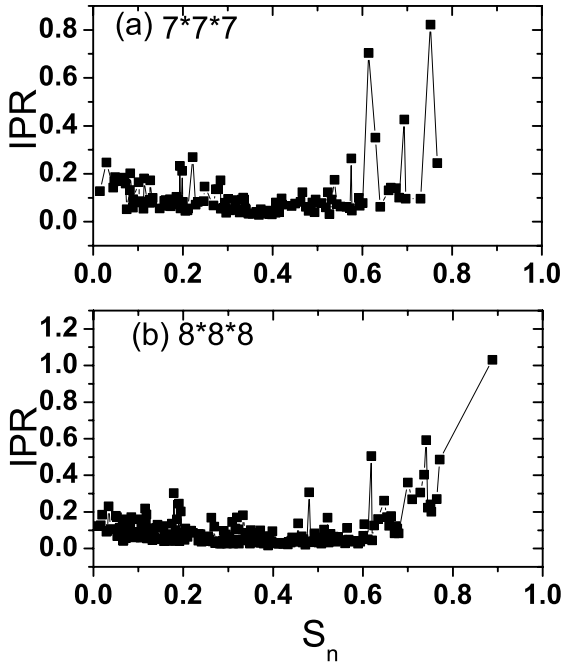

Fig. 6. Size effect of IPR of right eigenvectors at $p = 0.2$ in size (a) $7 \times 7 \times 7$ and (b) $8 \times 8 \times 8$.

reaches its maximum, and the density of states is larger around $s = 0.4$ than around $s = 0$ or $s = 1.0$. Therefore, considering randomicity, the size effect is not obvious in the distribution of IPR. Thus, the IPR in a finite size $8 \times 8 \times 8$ can be used to represent the properties of the local field of 3D disordered composites. While in 2D, according to reference [22], this size is 20×20.

Figure 7 displays the IPRs of 3D disordered composites with the concentration p varying from 0.2 to 0.4 and in size $8 \times 8 \times 8$. It is found that the localized states with the IPR values 0.2 or so and the extended states with very small IPR values are randomly distributed in the resonance regions. It is also shown that the intensity of IPR peaks varies little as p increases. There is a blue shift of IPR peak. But such a shift is not valid in the following effective linear optical responses.

As a comparison, we depict the IPRs of 2D composites in Figure 8 with p varying from 0.2 to 0.4 and in size 20×20. It is the same as that found in 3D, namely, the localized and extended states are randomly distributed in the whole resonance region [22]. However, there are some differences in IPR between 2D and 3D: in 3D, the blue shift of IPR peak is found with the increment of concentration, while in 2D, the positions of IPR peak are stable around $s = 0.83$. Comparing Figures 7 and 8, we also find that the states in 3D are more localized than that found in 2D. These differences originate from the different values of Green's function in 3D and 2D.

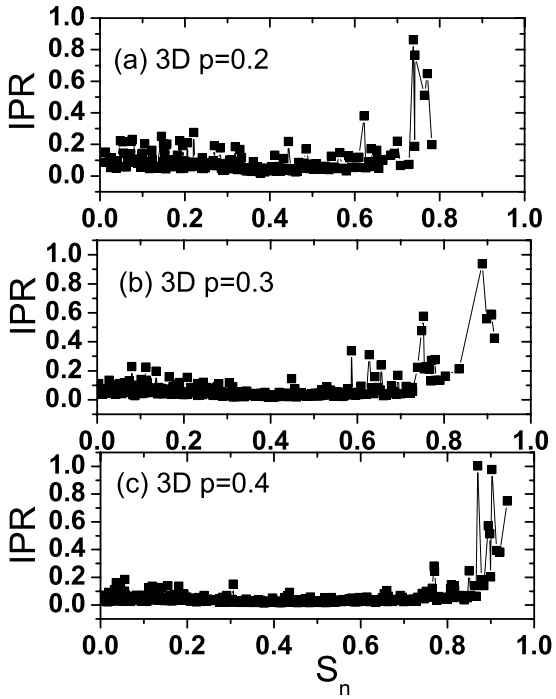

Fig. 7. IPR of right eigenvectors in 3D disordered composites with size $8 \times 8 \times 8$. (a) $p = 0.2$; (b) $p = 0.3$; (c) $p = 0.4$.

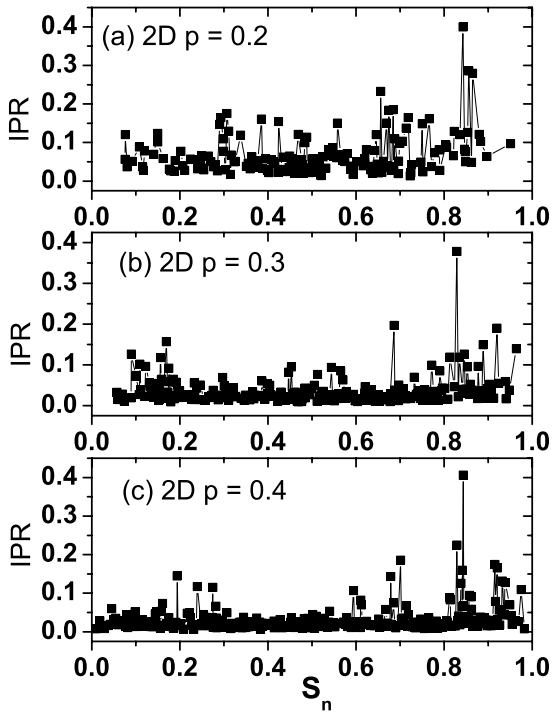

Fig. 8. IPR of 2D disordered composites with size 20×20. (a) $p = 0.2$; (b) $p = 0.3$; (c) $p = 0.4$.

5 Optical response of disordered isotropic composites

Consider a binary-composite network subject to a uniform field E_0 along 1 direction. With $E_0 = 1$, the admittance of each bond is generally complex and frequency-dependent, and the effective linear optical responses, namely, the absorption along the applied field can be represented by a bulk effective dielectric coefficient ϵ_e. According to

previous studies [13,22], the imaginary part of ϵ_e is:

$$\mathrm{Im}\,\epsilon_e = -\mathrm{Im}\sum_{n=1}^{n_s}\frac{\left(\sum_{\mathbf{y}\in\mathbf{C}} L_{n,\mathbf{y}\mathbf{y}_1}\right)\left(\sum_{\mathbf{x},\mathbf{y}\in\mathbf{C}}(x_1-y_1)(\tilde{R}_{n,\mathbf{x}}-\tilde{R}_{n,\mathbf{y}})\right)}{\epsilon_0(s-s_n)}, \tag{30}$$

$\mathbf{x},\mathbf{y}\in\mathbf{C}$ means $\mathbf{x}$ and $\mathbf{y}$ are the nearest neighbours in the same cluster, and $s=\frac{\epsilon_0}{\epsilon_0-\epsilon_1}$. When N_h represents the number of horizontal bonds along the applied field, the sum rule [13]

$$\sum_{n=1}^{n_s}\left(\sum_{\mathbf{y}\in\mathbf{C}} L_{n,\mathbf{y}\mathbf{y}_1}\right)\left(\sum_{\mathbf{x},\mathbf{y}\in\mathbf{C}}(x_1-y_1)\left(\tilde{R}_{n,\mathbf{x}}-\tilde{R}_{n,\mathbf{y}}\right)\right)=N_h, \tag{31}$$

is always obeyed and used to check the validity of the following computation. The Drude model is used to calculate the optical properties of three dimensional composites. The admittance ϵ_1 of the impurity metallic bonds is

$$\epsilon_1 = 1-\frac{\omega_p^2}{\omega(\omega+i\gamma)} \tag{32}$$

where ω_p is the plasma frequency, and γ a damping constant. For a metal, $\omega_p\approx 10^{16}$, lies in the ultraviolet. We choose $\gamma=0.01\omega_p$, which is the typical value for a metal. Let $\epsilon_0=1.77$, which is the dielectric constant of water for model calculations. The range of optical response is given by $\omega/\omega_p\in(0,1)$.

Figure 9 shows the imaginary parts (or absorption) of effective linear optical responses ϵ_e of 3D disordered composites per impurity bonds in a simple $14\times14\times14$ cubic lattice. For the volume fraction $p=0.10$, 0.15 and 0.20, the total number of bonds are 971, 1406 and 1842, respectively. There are two main absorption peaks always at resonances $s_n\approx0.20$ and 0.33, separated by a valley around $s_n\approx0.24$ for the different p. However, when $p=0.10$, the right peak is higher than the left one (Fig. 9a); when $p=0.15$, the two peaks are nearly at the same height (Fig. 9b); and the left peak is higher than the right one for $p=0.20$ (Fig. 9c). So there is a red shift of the absorption peaks with the increase of p, which agrees qualitatively with the Clausius-Mossotti (CM) approximation [18], i.e., the main peak is expected to be the value $s_n=(1-p)/d$, where d is the dimensionality. It is also noted that the peak around $s_n=0.33$ is just the position given by the CM approximation at $p\to0$, indicating the absorption property of homogeneous media. Hence the two methods give the same tendency. In Figure 9, it is also found that the whole absorption range broadens as p increases, namely, $0\sim0.7$ at $p=0.10$, and $0\sim0.8$ at $p=0.20$. It agrees with the results given by reference [31]. Moreover, as p increases from 0.1 to 0.2, the average contribution per impurity bond to the effective linear responses is approximately the same.

For comparison, we employ Figure 10 to display the effective linear optical responses per impurity bonds of

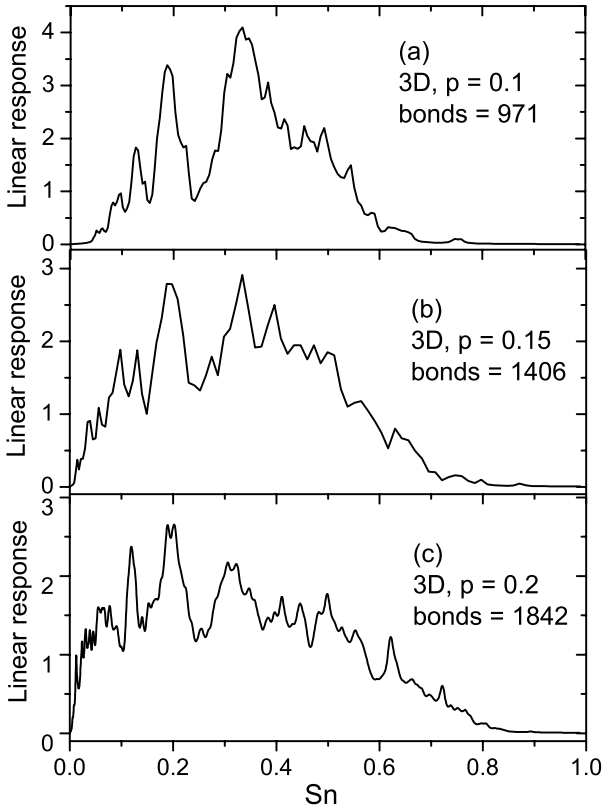

Fig. 9. Imaginary parts of the effective linear optical responses per impurity bond in 3D composites with size $14\times14\times14$. (a) $p=0.1$; (b) $p=0.15$; (c) $p=0.2$.

2D disordered composites in size 42×42. For $p=0.1$, 0.2 and 0.3, there are 371, 691 and 1075 impurity metallic bonds, respectively. The system shares many similar features with the 3D case, such as several main absorption peaks, the broadened absorption and effective linear responses of same order with increasing p. However, we have found several differences between 2D and 3D. There is one main peak localized around $s_n=0.5$ and two valleys around $s_n\approx0.4$ and $s_n\approx0.6$ regardless of the different volume fractions. And the main peak tends to split as p increases. Moreover, compared with 3D, more sub-peaks appear in 2D, as shown in Figures 10a, b and c.

6 Summary

In this paper, we have extended the electrostatic Green's function formalism to 3D. Using the formalism, we investigate the dielectric resonance, local field distribution near resonance, and effective optical responses in disordered 3D composites by the comparison with the corresponding 2D composites. For the same impurity metallic clusters, the values of the dielectric resonance in 3D are smaller than those in 2D. The sum rule of dielectric resonance in three-component composites becomes: $\sum s_m=\frac{n_2}{d}\eta+\frac{n_1}{d}$, where d is the degree of dimension, η the difference admittance ratio, and n_1 and n_2 the number of two kinds

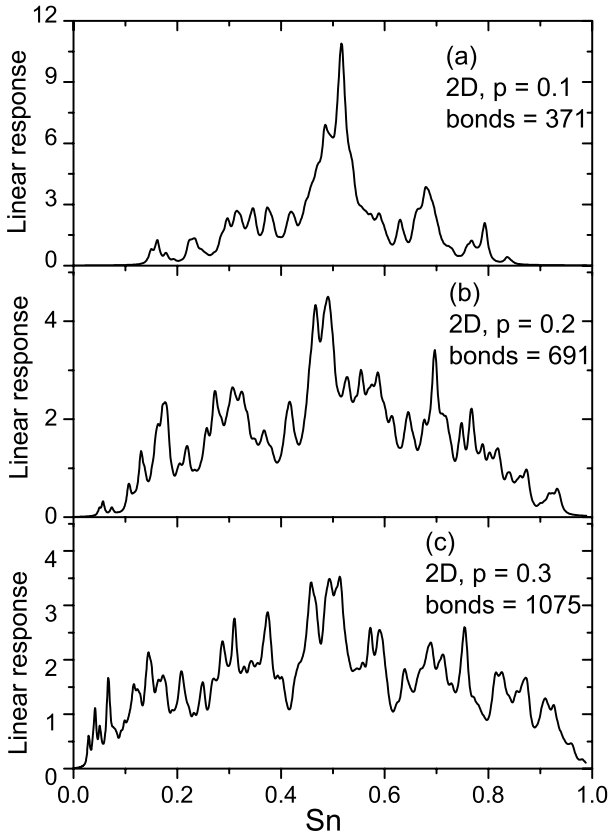

Fig. 10. Imaginary parts of the effective linear optical responses per impurity bond in 2D composites with size 42×42. (a) $p = 0.1$; (b) $p = 0.2$; (c) $p = 0.3$.

of impurity bonds with the admittance ϵ_1 and ϵ_2. For the same metallic cluster in both 3D and 2D, the local-field distribution near resonance has similar features, but the fields around the cluster in 3D are more localized than those in 2D. In the disordered 3D composites, we obtain a blue shift of IPR peaks with an increase of the impurity concentration, while, in 2D, we could not find this shift. Finally, the absorption range broadens with the increasing impurity concentration both for 2D and 3D disordered composites, a red shift of absorption peak is found in 3D as well.

The work was supported by National Natural Science Foundation of China under grant nos. 10304001, 10334010, 10328407, and 90101027. The work was also supported by the special fund from Ministry of Science and Technology of China, the National Key Basic Research Special Foundation under grant no. TG1999075207, and Junzheng Fund. We thank Profs. M.Z. Guo and C.S. Wu for stimulating and helpful discussions.

References

1. See article in *Nanostructured materials: Clusters, Composites and Thin Films,* edited by V.M. Shalaev, ACS Symposium Series 679 (American Chemical Society, Washington, D.C., 1997)
2. S.I. Bozhevolnyi, V.A. Markel, V. Coello, W. Kim, V.M. Shalaev, Phys. Rev. B **58**, 11441 (1998)
3. V.A. Markel, V.M. Shalaev, P. Zhang, W. Huynh, L. Tay, T.L. Haslett, M. Moskovits, Phys. Rev. B **59**, 10903 (1999)
4. A.K. Sarychev, V.A. Shubin, V.M. Shalaev, Phys. Rev. B **60**, 16389 (1999)
5. M.I. Stockman, S.V. Faleev, D.J. Bergman, Phys. Rev. Lett. **87**, 167401 (2001)
6. V.P. Safonov, V.M. Shalaev, V.A. Markel, Y.E. Danilova, N.N. Lepeshkin, W. Kim, S.G. Rautian, R.L. Armstrong, Phys. Rev. Lett. **80**, 1102 (1998)
7. M.I. Stockman, Phys. Rev. B **62**, 10494 (2000)
8. M.I. Stockman, Phys. Rev. E **56**, 6494 (1997)
9. R.P. Devaty, A.J. Sievers, Phys. Rev. Lett. **52**, 1344 (1984)
10. D.B. Tanner, A.J. Sievers, R.A. Buhrman, Phys. Rev. B **11**, 1330 (1975)
11. C.G. Granqvist, R.A. Buhrman, J. Wyns, A.J. Sievers, Phys. Rev. Lett. **37**, 625 (1976)
12. V.M. Shalaev, Phys. Rep. **27**, 61 (1996)
13. J.P. Clerc, G. Giraud, J.M. Luck, Th. Robin, J. Phys. A **29**, 4781 (1996)
14. M.I. Stockman, Phys. Rev. Lett. **84**, 1011 (2000)
15. M. Gadenne, V. Podolskiy, P. Gadenne et al., Europhys. Lett. **53**, 364 (2000)
16. V.M. Shalaev, A.K. Sarychev, Phys. Rev. B **57**, 13265 (1998)
17. D.J. Bergman, D. Stroud, in *Solid State Physics,* edited by H. Ehrenreich, D. Turnbull (Academic Press, New York, 1992), Vol. 146, p. 147
18. S. Kirkpatrick, Rev. Mod. Phys. **45**, 574 (1973)
19. Y. Gu, K.W. Yu, H. Sun, Phys. Rev. B **59**, 20 (1999)
20. Y. Gu, K.W. Yu, Z.R. Yang Phys. Rev. B **66**, 012202 (2002)
21. Y. Gu, Q.H. Gong, Phys. Rev. B **67**, 014209 (2003)
22. Y. Gu, K.W. Yu, Chin. Phys. **11**, 0601-07 (2002)
23. G. Albinet, L. Raymond, Eur. Phys. J. B **13**, 561 (2000)
24. D.J. Bergman, Y. Kantor, J. Phys. C: Solid State Physics, **14**, 3365 (1981)
25. F. Spitzer, *Principle of Ramdom Walk*, Graduate Texts in Mathematics, Vol. 34 (Berlin, Springer, 1976), pp. 78–80
26. J.D. Jackson, *Classical electrodynamics,* 2nd edn. (Wiley, New York, 1999), pp. 40–51
27. L. Raymond, J.-M. Laugier, S. Schäfer, G. Albinet, Eur. Phys. J. B **31**, 355 (2003)
28. Y. Gu, Q.H. Gong, Phys. Rev. B **69**, 035105 (2004)
29. M.F. Law, Y. Gu, K.W. Yu, J. Phys.: Condens. Matter **10**, 9549 (1998)
30. F. Wegner, Z. Phys. B **36**, 209T (1980)
31. N.E. Russell, E.M. Yam, D.B. Tanner, in *Electrical Transport and Optical Properties of Inhomogeneous Media*, edited by J.C. Garland, D.B. Tanner, AIP Conf. Proc. No. **40**, 258 (1978)